Asian Research Journal of Mathematics

14(4): 1-17, 2019; Article no.ARJOM.50499

ISSN: 2456-477X

Keller-box Study on Casson Nano Fluid Flow over a Slanted Permeable Surface with Chemical Reaction

Khuram Rafique[1*], Muhammad Imran Anwar[2,3] and Masnita Misiran[1]

[1]School of Quantitative Sciences, Universiti Utara Malaysia, 06010, Sintok, Kedah, Malaysia.
[2]Department of Mathematics, Faculty of Science, University of Sargodha, Pakistan.
[3]Higher Education Department (HED), Punjab, Pakistan.

Authors' contributions

This work was carried out in collaboration among all authors. Author KR designed the study, performed the statistical analysis, wrote the protocol and wrote the first draft of the manuscript. Author MIA managed the analyses of the study. Author MM managed the literature searches. All authors read and approved the final manuscript.

Article Information

DOI: 10.9734/ARJOM/2019/v14i430135
Editor(s):
(1) Dr. Wei-Shih Du, Professor, Department of Mathematics, National Kaohsiung Normal University, Taiwan.
Reviewers:
(1) Fateh Mebarek-Oudina, Skikda University, Algeria.
(2) Rajib Biswas, Bangladesh University, Bangladesh.
Complete Peer review History: http://www.sdiarticle3.com/review-history/50499

Original Research Article

Received: 14 May 2019
Accepted: 26 July 2019
Published: 01 August 2019

Abstract

In this problem, an examination of Casson Nanofluid boundary layer flow over linear slanted extending sheet by fusing the chemical reaction and heat generation impacts are under thought. Nanofluid demonstrate in this examination is developed on Buongiorno model for the thermal efficiencies of the liquid flow in the presence of Brownian movements and thermophoresis impacts. The nonlinear issue for Casson Nanofluid flow over slanted channel is displayed to ponder the heat and mass exchange wonder by considering portant flow parameters to strengthen the boundary layers. The governing nonlinear partial differential equations are decreased to nonlinear normal differential equations and afterward illustrated numerically by methods for the Keller-Box plot. An examination of the set up results in the absence of the joined impacts is performed with the accessible outcomes of Khan and Pop [1] and set up in a decent contract. Numerical and graphical outcomes are additionally exhibited in tables and graphs.

Keywords: Casson Nano fluid; chemical reaction; heat generation/absorption; inclined surface.

**Corresponding author: E-mail: Khurram.rafique1005@gmail.com;*

Nomenclature

g	*: Acceleration due to gravity*
B_0	*: Uniform magnetic field strength*
σ	*: Electrical conductivity*
μ	*: Viscosity*
δ_f	*: Density of the base fluid*
δ_p	*: Density of the nanoparticle*
β	*: Casson parameter*
β_t	*: Coefficient of thermal expansion*
β_c	*: Coefficient of concentration expansion*
D_B	*: Brownian diffusion coefficient*
D_T	*: Thermophoresis diffusion coefficient*
k	*: Thermal conductivity*
$(\delta c)_p$	*: Heat capacitance of the nanoparticles*
$(\delta c)_f$	*: Heat capacitance of the base fluid*
$\alpha = \frac{k}{(\delta c)_f}$	*: Thermal diffusivity parameter*
S	*: Suction parameter*
M	*: Magnetic parameter called Hartmann number*
ν	*: Kinematic viscosity of the fluid*
Pr	*: Prandtl number*
Le	*: Lewis number*
$-\theta'(0)$	*: Reduced Nusselt number*
$-\phi'(0)$	*: Reduced Sherwood number*
C_{fx}	*: Skin friction coefficient*
$Re = \frac{u_w x}{\nu}$	*: Local Reynolds number*
Nb	*: Brownian motion parameter*
Nt	*: Thermophoresis parameter*
λ	*: Buoyancy parameter*
δ	*: Solutal buoyancy parameter*
γ	*: Inclination parameter*
λ_1	*: Heat generation or absorption parameter*
R	*: Chemical reaction parameter*
$\tau = \frac{(\delta c)_p}{(\delta c)_f}$	*: Ratio between the effective heat capacity of the nanoparticle and heat capacity of the fluid*

1 Introduction

In the prior couple of decades, quick advances in nanotechnology have prompt creating of new-age coolants called "Nano liquid". Nano liquids are potential heat exchange fluids with improved thermo physical properties and heat trade execution can be associated with various tools for better exhibitions (for example imperativeness, heat exchange, and other performances). Nano liquids are structured by interfering with nanoparticles with typical sizes underneath 100 nm in ordinary heat transfer liquids, for example, oil, water, and ethylene glycol. These are current heat exchange masters that trigger the thermal conductivity of the base liquids and an important subject for specialists and scientists for the most recent couple of years because of its varied development and current applications Choi [2]. Eastman et al. [3] inspected in an investigation when nanoparticles are included base liquid (water) with a volume portion 5% the thermal conductivity upgraded up to 60%. Moreover, Eastman et al. [3] announced that the thermal conductivity expanded up to 40% by including the copper nanoparticles with volume part 1% in the customary liquid ethylene glycol or oil. Buongiorno [4] has talked about in his investigation there are seven systems, which are imperative to upgrade the thermal conductivity of the base liquid. Among all these Brownian movement and thermophoresis are increasingly significant. Anwar et al. [5] studied the numerical study of micropolar nanofluid flow over a stretching sheet. Mitra [6] investigated computational modeling of nanofluid flow over a heated inclined plate. Khan et al. [7] illustrated the heat and mass transfer of MHD Jeffery nanofluid flow over an inclined sheet. Hatami et al. [8] discussed three-dimensional steady nanofluid over an inclined disk. Govindrajan [9] investigated the nanofluid flow over a slanted sheet. Nanofluid flow with radiation effects on a slanted surface examined by Chakraborty [10]. Besides, the similarity solution of nanofluid on the permeable sheet studied by Ziaei-Rad et al. [11]. Thumma et al. [12] discussed the nanofluid flow on a slanted plate by incorporating the heat source. For more literature about nanofluids flow against different geometries we can see [13-18].

Casson fluid is a shear thinning liquid which should have zero viscosity at an infinite measure of shear and infinite viscosity at zero degree of shear, yield stress under which no flow occurs. Shear thinning states the response of a liquid substance thickness when force applied. The examples of Casson liquid are jam, tomato glue, stock, thorough organic product fluids, and human blood and so on Kumar et al. [19]. Casson liquid stream assumes a key job in designing. Shaw et al. [20] discussed the effect of different parameters on Casson fluid stream over a plate with convective farthest point conditions at surface. Ali et al. [21] discussed the Casson fluid flow over a slanted sheet. Casson fluid flow over a slanted plate calculated by Vijayaragavan and Kavitha [22]. Shamshuddin et al. [23] numerically investigated the effect of chemical reaction on Casson fluid flow on a slanted plate. Casson fluid is more useful cooling agent as compere to other fluids [24-30].

The heat and mass exchange with chemical reaction over a slanted extending plate has achieved a significant intrigue as a result of its various applications in building. Anwar et al. [31] examined the MHD stagnation point flow of nanofluid flow over a sheet. shit and Majee [32] expounded the impacts of chemical reaction on magnetohydrodynmaic fluid flow over nonlinear extending slanted surface. Mixed convection flow over a vertical plate by joining impacts of chemical reaction and heat generation examined by Eid [33]. Malik [34] talked about MHD two dimensional flow over penetrable slanted surface with second order chemical reaction. Jain and Bohra [35] examined the impact of chemical reaction on three dimensional incompressible flows over a slanted surface. Heat and mass exchange MHD free convection flow over a slanted plate inspected by Sheri and Modugula [36]. For further literature regarding heat and mass exchange with different impacts, we can see [37-41].

Motivated by the earlier cited literature, we decide to work on Casson nanofluid flow on a slanted Permeable stretching surface with chemical reaction and heat generation. Although, a lot of work already done on non-Newtonian fluid with different effects due to its increasing need in the industry and engineering field we develop the understudy model. We use Keller-box method for the numerical solution after converting the nonlinear partial differential equations into nonlinear ordinary differential equations. According to the author's best knowledge, all the results are new.

2 Problem Formulation

A steady, two dimensional boundary layer flow of Casson Nano fluid on a porous slanted linear enlarging plate with an angle γ is under account. The extending and free stream speeds are supposed to stand as, $u_w(x) = ax$ and $u_\infty(x) = 0$ respectively, here 'x' is the coordinate dignified along the extending surface and 'a' is a constant. The Brownian motion and thermophoresis properties are taken into account. The temperature T and Nano particle fraction C take the constant values T_w and C_w on the wall, on the other hand ambient forms for nanofluid temperature and mass fractions T_∞ and C_∞ are attained as y inclines to immensity shown in Fig. 1.

The subjected governing equations are:

$$\frac{\partial u}{\partial x} + \frac{\partial v}{\partial y} = 0 \tag{1}$$

$$u\frac{\partial u}{\partial x} + v\frac{\partial u}{\partial y} = \nu(1 + \frac{1}{\beta})\frac{\partial^2 u}{\partial y^2} + g[\beta_t(T - T_\infty) + \beta_c(C - C_\infty)]cos\gamma - \sigma {B_0}^2(x)u \tag{2}$$

$$u\frac{\partial T}{\partial x}+v\frac{\partial T}{\partial y}= \alpha\frac{\partial^2 T}{\partial y^2}+\tau\left[D_B\frac{\partial C}{\partial y}\frac{\partial T}{\partial y}+\frac{D_T}{T_\infty}\left(\frac{\partial T}{\partial y}\right)^2\right]+\frac{Q_0}{\delta C_p}(T-T_\infty) \tag{3}$$

$$u\frac{\partial C}{\partial x}+v\frac{\partial C}{\partial y}=D_B\frac{\partial^2 C}{\partial y^2}+\frac{D_T}{T_\infty}\frac{\partial^2 T}{\partial y^2}+R^*(C-C_\infty) \tag{4}$$

Where u and v are the components of velocity in x and y directions, respectively, g is the acceleration due to gravity, B_0 is the uniform magnetic field strength, σdenotes the electrical conductivity, μ is the viscosity, δ_f is the density of the improper liquid, δ_p denotes density of the nanoparticle, β_t is the factor of thermal extension, β_c denote the factor of concentration enlargement, D_B denote the Brownian diffusion factor and D_T denotes the thermophoresis diffusion factor, Q_0 is the heat generation or absorption coefficient, R^* is the chemical reaction coefficient,$(\delta c)_p$denotes the heat capacitance of the nanoparticles, $(\delta c)_f$ represents the heat capacitance of the improper liquid, thermal diffusivity parameter is denoted by $\alpha=\frac{k}{(\delta c)_f}$ and the ratio between the effective heat capacity of the nanoparticle and heat capacity of the liquid is represented by $\tau=\frac{(\delta c)_p}{(\delta c)_f}$.

The subjected boundary conditions are

$$\begin{aligned}&u=u_w(x)=ax, v=V_w\,, T=T_w\,, C=C_w \quad at \quad y=0,\\ &u\to u_\infty(x)=0, v\to 0\,, T\to T_\infty\,, C\to C_\infty \quad at \quad y\to\infty,\end{aligned} \tag{5}$$

Here we obtained nonlinear ordinary differential equations from nonlinear partial differential equations by using stream function $\psi=\ \psi(x,y)$ demarcated as

$$u=\frac{\partial\psi}{\partial y},\ \ v=-\frac{\partial\psi}{\partial y}, \tag{6}$$

Where equation (1) is fulfilled identically. The similarity transformations are demarcated as

$$\begin{aligned}&u=axf'(\eta), v=-\sqrt{av}f(\eta), \eta=y\sqrt{\frac{a}{v}}\\ &\theta(\eta)=\frac{T-T_\infty}{T_w-T_\infty}, \phi(\eta)=\frac{C-C_\infty}{C_w-C_\infty},\end{aligned} \tag{7}$$

On substituting equation (7), system of equations (2-4) reduces to the following nonlinear ordinary differential equations:

$$(1+\frac{1}{\beta})f'''+ff''-f'^2+(\lambda g+\delta q)cos\gamma-Mf'=0 \tag{8}$$

$$\left(\frac{1}{Pr}\right)\theta''+f\theta'+\lambda_1\,\theta'+Nb\phi'\theta'+Nt\theta'^2=0 \tag{9}$$

$$\phi''+Lef\phi'+Nt_b\theta''-LeR\phi=0 \tag{10}$$

Where

$$\begin{aligned}&\lambda=\frac{Gr_x}{Re_x}, \delta=\frac{Gc}{Re_x}, M=\frac{\sigma B^2(x)}{a\rho}, Le=\frac{v}{D_B}, Pr=\frac{v}{\alpha}, N_b=\frac{\tau D_B(C_w-C_\infty)}{v}, N_t=\frac{\tau D_t(T_w-T_\infty)}{vT_\infty},\\ &Gr_x=\frac{g\beta_t(T_w-T_\infty)x}{av}, Re_x=\frac{u_w(x)x}{v}, Gc_x=\frac{g\beta_c(C_w-C_\infty)x}{av},\ Nt_b=\frac{N_t}{N_b}, \lambda_1=\frac{Q_0}{a\rho c_p}, R=\frac{R^*}{a},\end{aligned} \tag{11}$$

Here, primes denotes the differentiation with respect to η, λ Buoyancy parameter, δ Solutal buoyancy parameter, M is the magnetic constraint, v denotes the kinematic viscidness of the liquid, Pr denotes the Prandtl number, Le denotes the Lewis number, Chemical reaction parameter is denoted by R, λ_1 Heat generation or absorption parameter.

The equivalent boundary settings are converted to

$$f(\eta) = S,\ \ f'(\eta) = 1,\ \theta(\eta) = 1,\ \phi(\eta) = 1 \ \ at\ \eta = 0,$$
$$f'(\eta) \to 0,\ \ \theta(\eta) \to 0,\ \phi(\eta) \to 0\ as\ \ \eta \to \infty, \tag{12}$$

The skin friction, Sherwood number and Nusselt number for the current study are defined as

$$Nu_x = \frac{xq_w}{k(T_w - T_\infty)},\ Sh_x = \frac{xq_m}{D_B(C_w - C_\infty)},\ C_f = \frac{t_w}{{u_w}^2 \rho_f}, \tag{13}$$

The reduced Sherwood number $-\phi'(0)$, skin-friction coefficient $C_{fx}(0) = f''(0)$, and the reduced Nusselt number $-\theta(0)$, are demarcated as

$$-\theta'(0) = \frac{Nu_x}{\sqrt{Re_x}},\ -\phi'(0) = \frac{Sh_x}{\sqrt{Re_x}}, C_{fx} = C_f\sqrt{Re_x}, \tag{14}$$

Where, $Re_x = \frac{u_w(x)x}{\nu}$ is the local Reynolds number

The converted nonlinear differential equations (8-10) with the boundary conditions (12) are elucidated by Keller box method consisting on the steps as, finite-differences technique, Newton's scheme and block elimination process clearly explained by Anwar et al. [5].

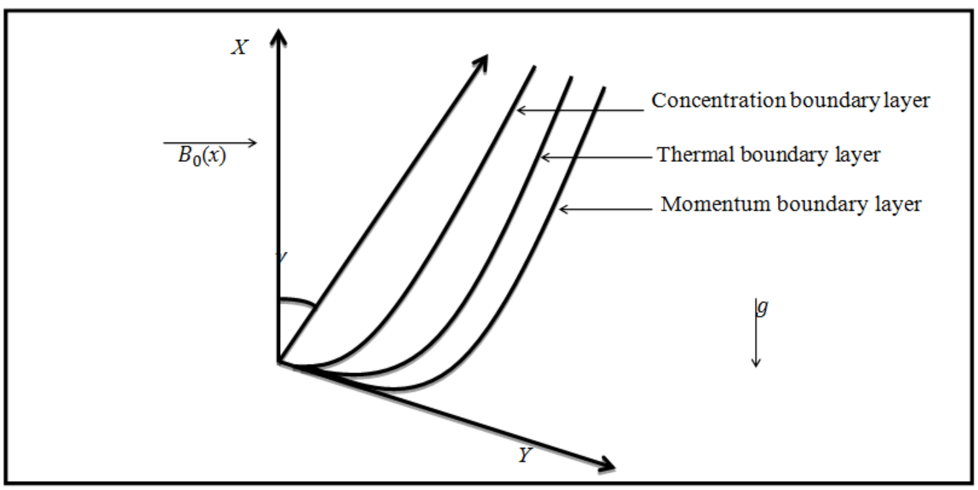

Fig. 1. Physical geometry with coordinate system

3 Results and Discussion

The transformed nonlinear ordinary differential equations (8-10) with boundary conditions (12) are solved via Killer-box method. For numerical result of physical parameters of our concern including Brownian motion parameter Nb, thermophoresis parameter Nt, Chemical reaction constraint R, magnetic factor M, buoyancy constraint λ, heat generation or absorption bound $\lambda 1$, solutal buoyancy constraint δ, inclination parameter γ, Casson fluid parameter β, Prandtl number Pr, Lewis number Le, and suction parameter S, several Figures and Tables are prepared. In Table 3.1, in the absence of buoyancy parameter λ, solutal buoyancy parameter δ, with γ = 90° when Casson constraint $\beta \to \infty$ outcomes for reduced Nusselt number $-\theta'(0)$, reduced Sherwood number $-\phi'(0)$ are equated with the existing outcomes of Khan and Pop [1]. The fallouts are established brilliant settlement. The effects of reduced Nusselt number $-\theta'(0)$, reduced

Sherwood number $-\phi'(0)$ and skin friction coefficient $C_{fx}(0)$ against different values of involved physical parameters Nb, β, Nt, R, M, $\lambda 1$, λ , δ,γ, Pr, Le and S are shown in Table 3.2. It is noted that $-\theta'(0)$ decreases for increasing the values of Nb, β, γ, Nt, M, $\lambda 1$, Le, Pr, S and increased by increasing the numerical values of , R, λ, δ and for decreasing values of S. Moreover, it is observed that $-\phi'(0)$ enhanced with the larger values of Nb, Pr, Nt, Le, $\lambda 1$, λ, δ and for small values of S. It is true physically, which results in enhanced the Brownian parameter the movement of the fluid particles enhanced due to which the thermal boundary layer thickness. Whereas, decreases for cumulative the values of R, γ, M and S. On the other hand, $C_{fx}(0)$ surges with the increasing values of Nb, Le, M, β, $\lambda 1$, γ and for small values of S. Moreover, decreases with the increasing values of Nt, λ, δ, Pr, R and S.

Fig. 2 depicts the effect of magnetic field parameter on velocity profile. It is found that the velocity profile decreases for bigger values of magnetic field parameter M. It is due to the application of magnetic field produces Lorentz force, by means slow down the speed of the fluid. Moreover, Figs. 3 and 4 present the temperature and concentration contours increase by enhancing the values of M.

The effects of suction parameter S on the velocity profile are shown in Fig. 5. It is perceived that the velocity profile decline by growing the suction parameter signifying the normal fact that suction steadies the boundary layer development due to which the creation of highest in the velocity outline also drops. Besides, the same effect showed in the case of temperature profile and concentration profile respectively in Figs. 6 and 7.

Table 3.1. Contrast of the reduced Nusselt number $-\theta'(0)$ and the reduced Sherwood number $-\phi'(0)$ with M, δ, S, R, λ_1, $\lambda = 0$, Pr = Le = 10 and γ= 90° when $\beta \to \infty$.

Nb	*Nt*	Khan and Pop [1]		Current Outcomes	
		$-\theta'(0)$	$-\phi'(0)$	$-\theta'(0)$	$-\phi'(0)$
0.1	0.1	0.9524	2.1294	0.9524	2.1294
0.2	0.2	0.3654	2.5152	0.3654	2.5152
0.3	0.3	0.1355	2.6088	0.1355	2.6088
0.4	0.4	0.0495	2.6038	0.0495	2.6038
0.5	0.5	0.0179	2.5731	0.0179	2.5731

Table 3.2 Outcomes of the reduced Nusselt number $-\theta'(0)$, the reduced Sherwood number $-\phi'(0)$ and the Skin-friction coefficient $C_{fx}(0)$

Nb	*Nt*	Pr	*Le*	*M*	*β*	*R*	*λ 1*	*λ*	*δ*	*S*	*γ*	$-\theta'(0)$	$-\phi'(0)$	$C_{fx}(0)$
0.1	0.1	6.5	5.0	0.5	1.0	1.0	0.1	0.1	0.9	0.1	45^0	0.7385	0.7248	0.6709
0.3	0.1	6.5	5.0	0.5	1.0	1.0	0.1	0.1	0.9	0.1	45^0	0.2942	0.9897	0.6978
0.1	**0.3**	6.5	5.0	0.5	1.0	1.0	0.1	0.1	0.9	0.1	45^0	0.4591	0.9008	0.6139
0.1	0.1	**10.0**	5.0	0.5	1.0	1.0	0.1	0.1	0.9	0.1	45^0	0.6977	0.8104	0.6703
0.1	0.1	6.5	**10.0**	0.5	1.0	1.0	0.1	0.1	0.9	0.1	45^0	0.6220	1.5163	0.7203
0.1	0.1	6.5	5.0	**2.0**	1.0	1.0	0.1	0.1	0.9	0.1	45^0	0.6911	0.5356	1.0322
0.1	0.1	6.5	5.0	0.5	**5.0**	1.0	0.1	0.1	0.9	0.1	45^0	0.7183	0.6520	0.8109
0.1	0.1	6.5	5.0	0.5	1.0	**2.0**	0.1	0.1	0.9	0.1	45^0	1.1379	-2.3869	0.5423
0.1	0.1	6.5	5.0	0.5	1.0	1.0	**0.5**	0.1	0.9	0.1	45^0	-0.2881	1.5280	0.6821
0.1	0.1	6.5	5.0	0.5	1.0	1.0	0.1	**1.0**	0.9	0.1	45^0	0.7504	0.7570	0.5565
0.1	0.1	6.5	5.0	0.5	1.0	1.0	0.1	0.1	**3.0**	0.1	45^0	0.7736	0.8445	0.3438
0.1	0.1	6.5	5.0	0.5	1.0	1.0	0.1	0.1	0.9	**0.3**	45^0	0.3124	0.5246	0.6032
0.1	0.1	6.5	5.0	0.5	1.0	1.0	0.1	0.1	0.9	**0.0**	45^0	0.9988	0.8108	0.7060
0.1	0.1	6.5	5.0	0.5	1.0	1.0	1.0	1.0	1.0	**-0.3**	45^0	1.9229	1.0041	0.8114
0.1	0.1	6.5	5.0	0.5	1.0	1.0	1.0	1.0	1.0	0.1	**60^0**	0.7334	0.7015	0.7191

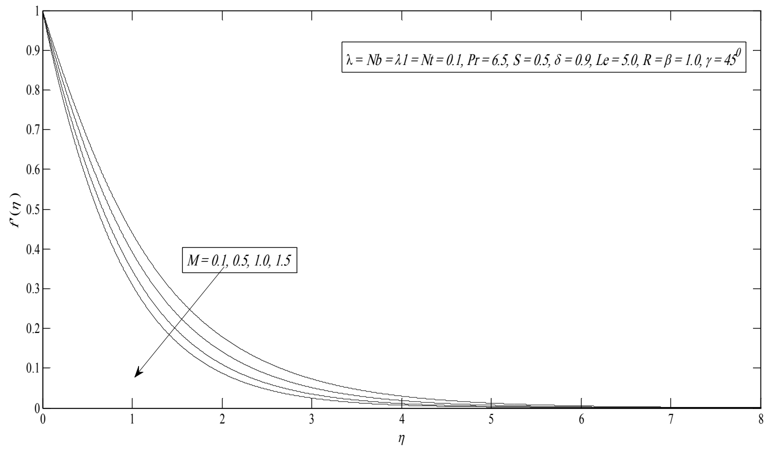

Fig. 2. Velocity profile for several values of *M*

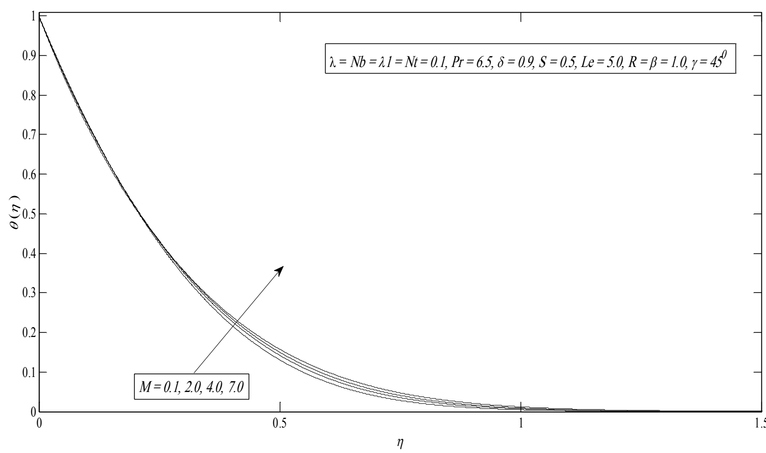

Fig. 3. Temperature profile for several values of *M*

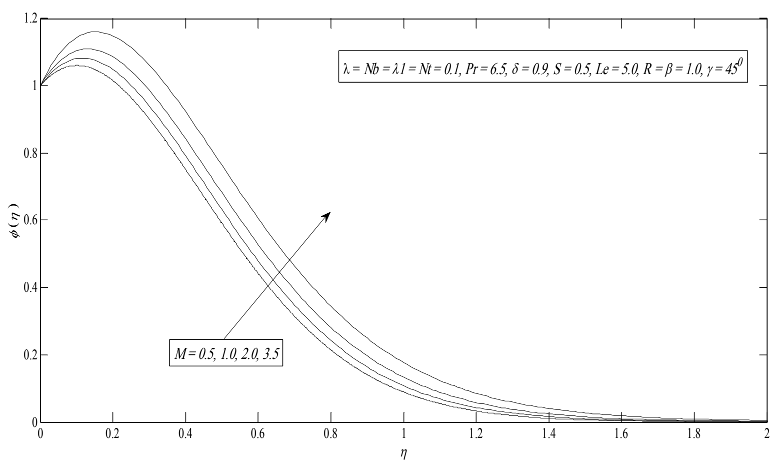

Fig. 4. Concentration profile for several values of *M*

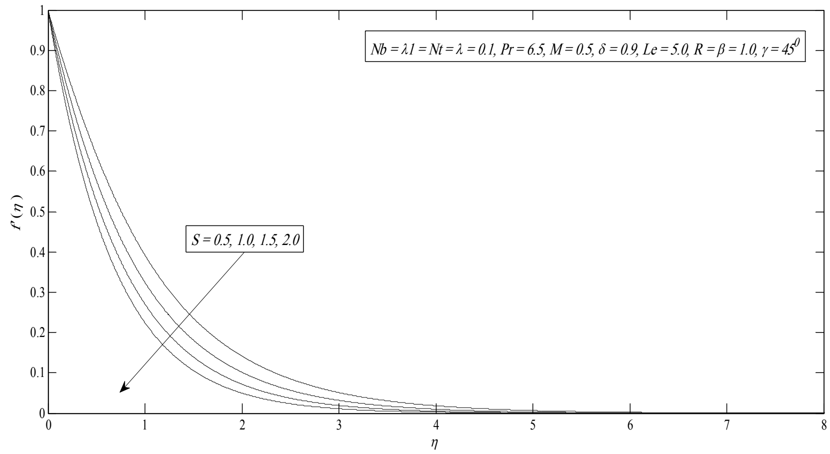

Fig. 5. Velocity profile for several values of *S*

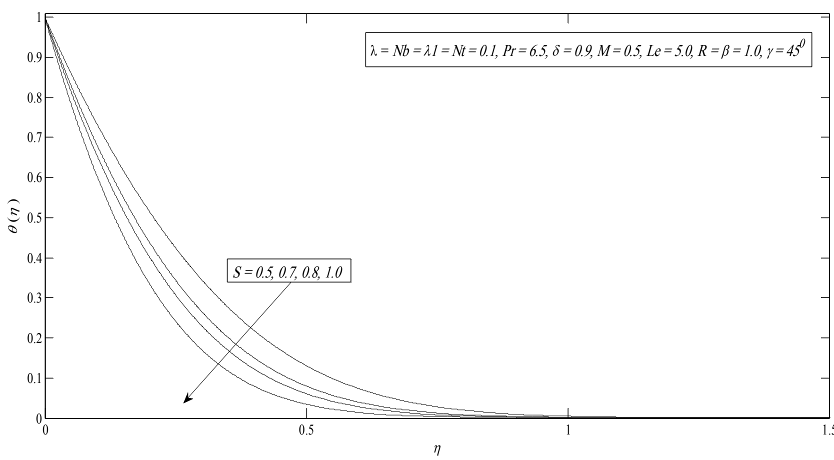

Fig. 6. Temperature profile for several values of *S*

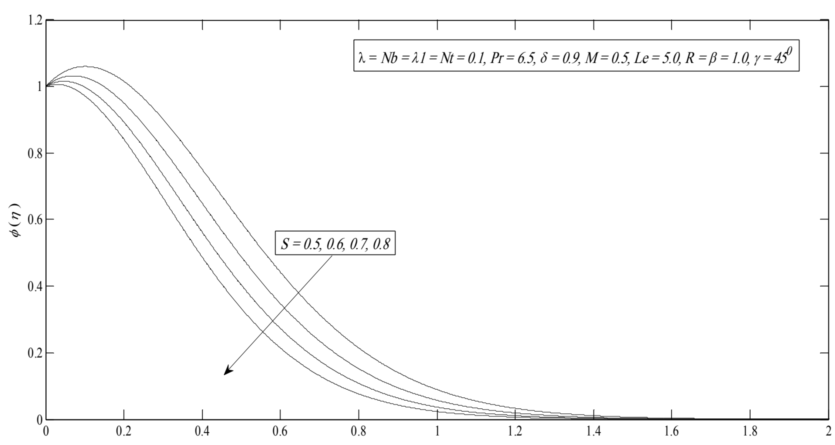

Fig. 7. Concentration profile for several values of *S*

The outcome of Casson constraint on velocity factor is presented in Fig. 8. It is detected that for different values of Casson parameter velocity profile decreases. The cause overdue this behavior is that by growing the values of Casson parameter β increases the fluid viscosity i.e. falling the yield stress. Therefore, the momentum boundary layer thickness reduces. The impacts of buoyancy factor are shown in Fig. 9. It is pragmatic that the velocity profile rise by improving the buoyancy limit. Fig. 10 indicates that the velocity outline increases by enhancing the solutal buoyancy factor.

Fig. 11 indicates that the velocity profile decelerated by enhancing the values of the inclination parameter γ. This is because of enhancing the value of the inclination parameter; retard the strength of the bouncy force by a factor $cos\gamma$ because of the thermal variation. Also we found that the influence of the bouncy force (which is highest for $\gamma = 0$) exceeds the main stream velocity significantly. The same impact indicates in Fig. 12 for temperature profile but opposite impact presents in the case of concentration profile in Fig. 13.

Figs. 14 and15 indicate the effect of Brownian cue on the temperature and concentration outlines. The temperature contour enlarges by enhancing the Brownian motion. Moreover, contrary style is seen beside the concentration outlines. Substantially, the enlargement in Brownian movement factor supports to heat up the boundary layer which inclines to travel nanoparticles from the extending sheet to the motionless liquid. Therefore the concentration nanoparticle moderates. Moreover, Figs. 16 and 17 specify the effects of thermophoresis parameter on temperature and concentration contours. It is found that mutually temperature and concentration profiles are increases for large values of thermophoresis parameter Nt.

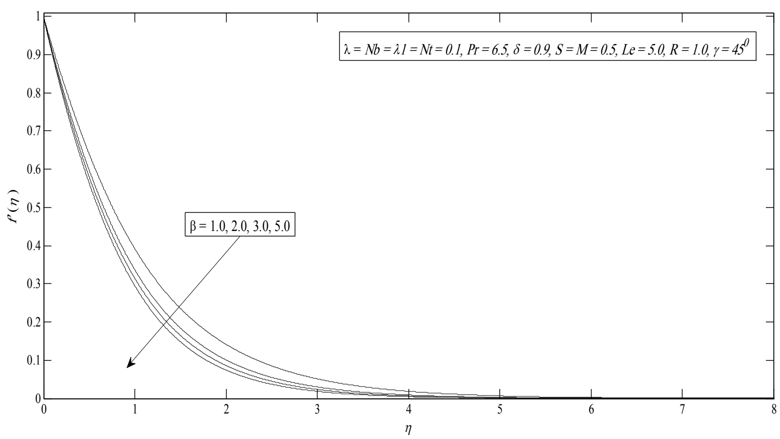

Fig. 8. Velocity profile for several values of $\boldsymbol{\beta}$

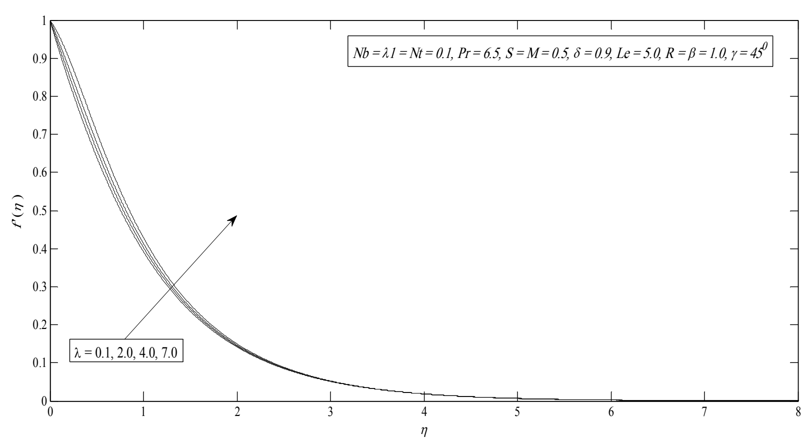

Fig. 9. Velocity profile for several values of $\boldsymbol{\lambda}$

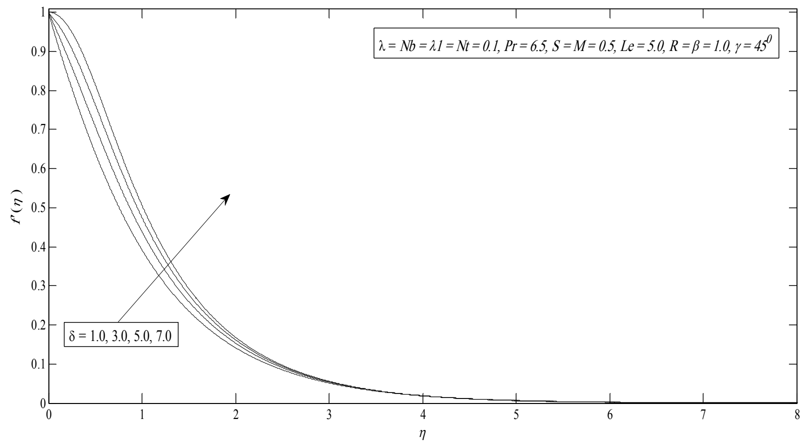

Fig. 10. velocity profile for several values of δ

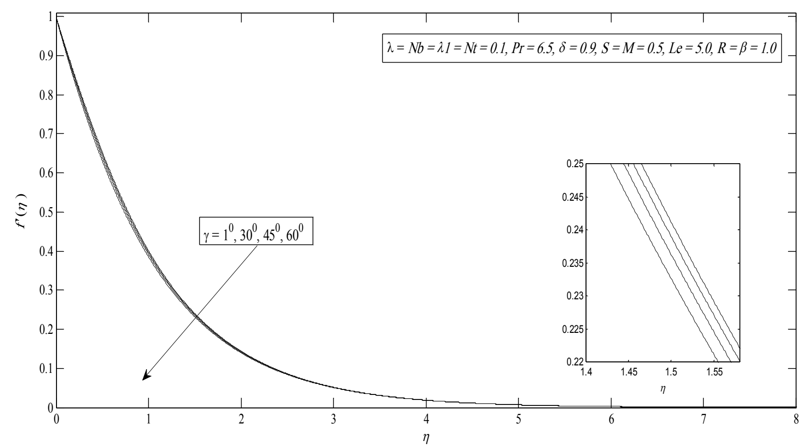

Fig. 11. Velocity profile for several values of γ

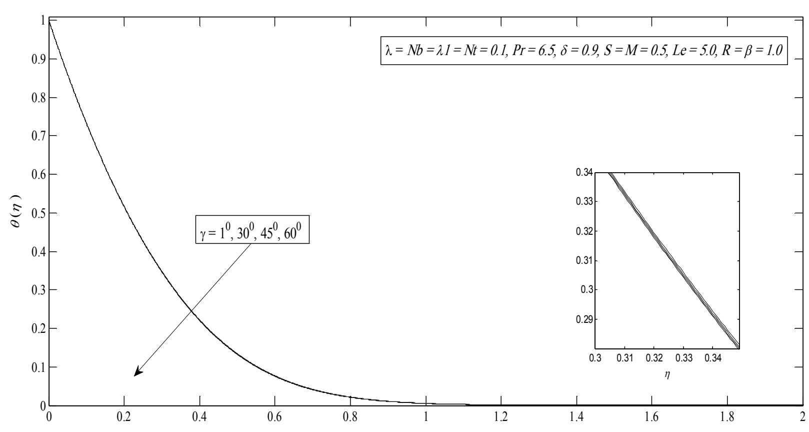

Fig. 12. Temperature profile for several values of γ

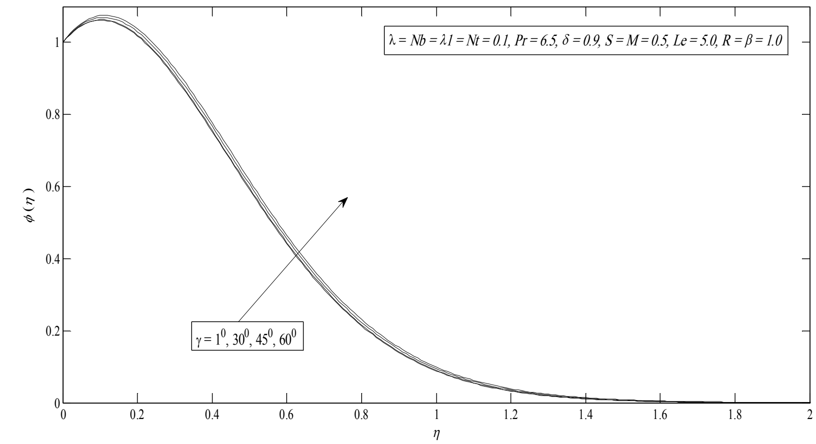

Fig. 13. Concentration profile for several values of γ

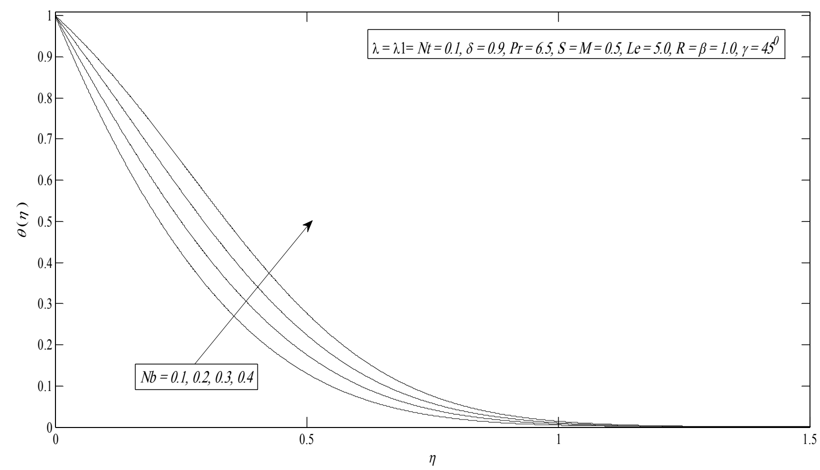

Fig. 14. Temperature profile for several values of Nb

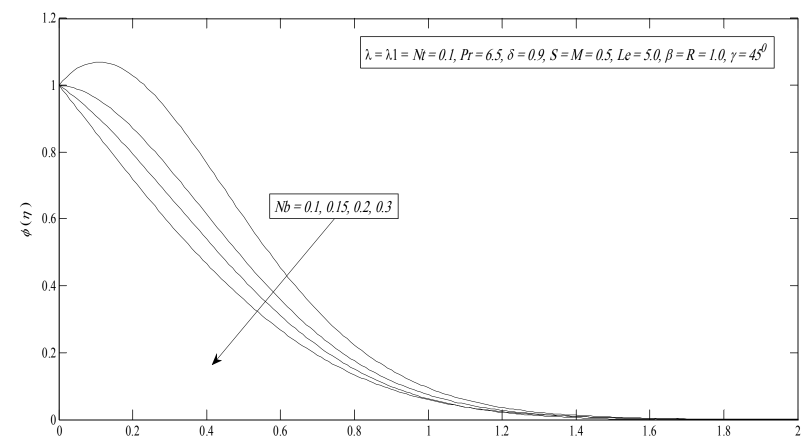

Fig. 15. Concentration profile for several values of Nb

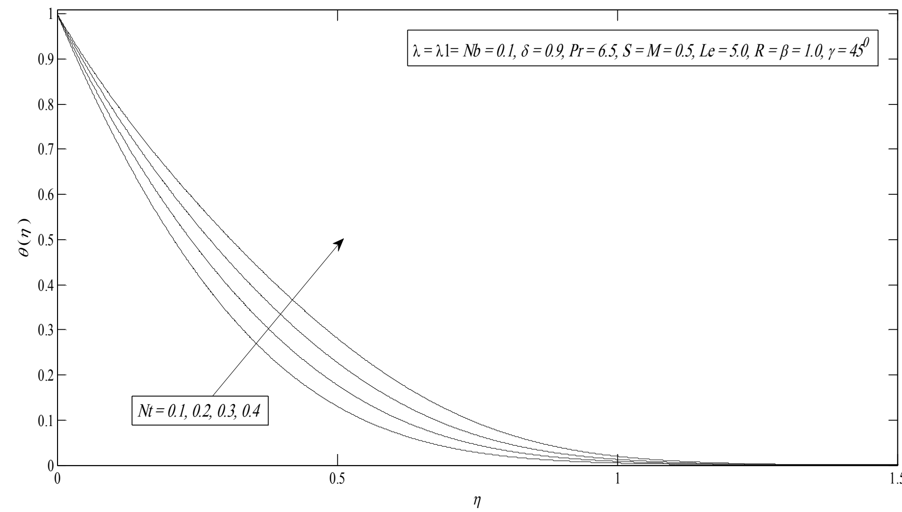

Fig. 16. Temperature profile for several values of Nt

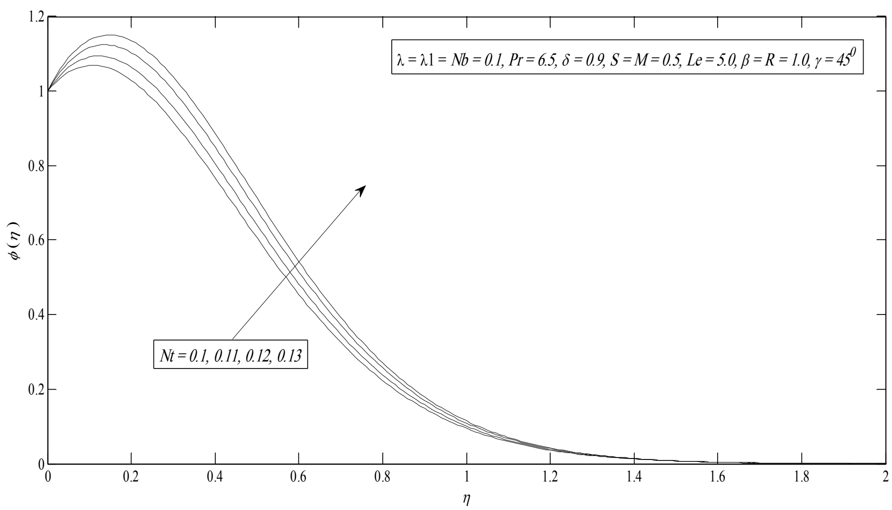

Fig. 17. Concentration profile for several values of Nt

Figs. 18 and 19 depict the effect of Prandtl number Pr on temperature and Lewis number Le on concentration profile. It indicates that the temperature profile decrease for large values of Prandtl number. The boundary layer thickness shortens by enhancing the values of Prandtl number. Moreover, the concentration profile decrease for higher values of Lewis number Le which shows Lewis number reduces the boundary layer thickness.

Figs. 20 and 21 presented the effect of heat generation on temperature and chemical reaction on concentration outline. It is noted that the temperature and concentration contour upsurge by growing the values of heat generation constraint λ_1 and chemical reaction constraint R. The velocity of the liquid enhance by increasing the values of heat generation, due to which heat generate in the flow region and the temperature increase with in the thermal boundary layer.

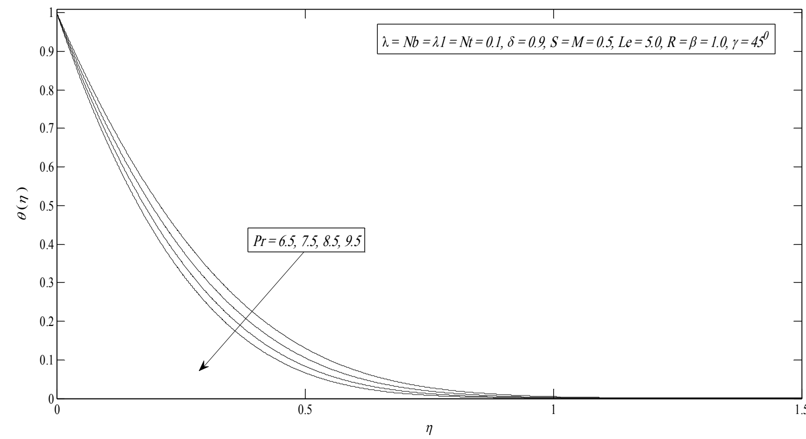

Fig. 18. Temperature profile for several values of Pr

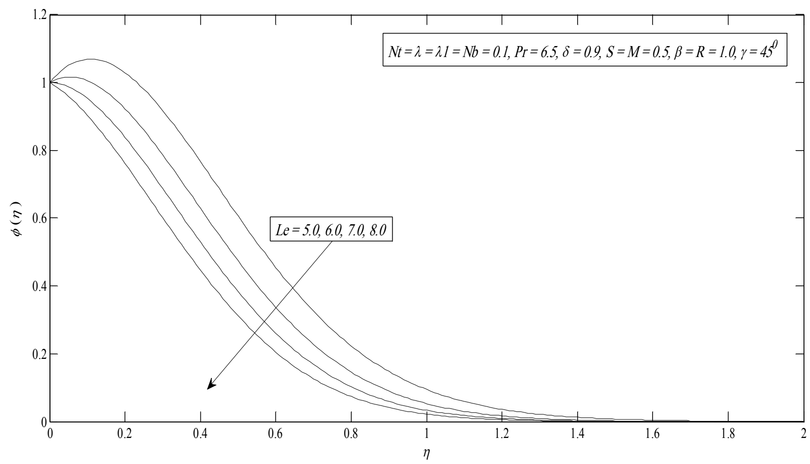

Fig. 19. Concentration profile for several values of Le

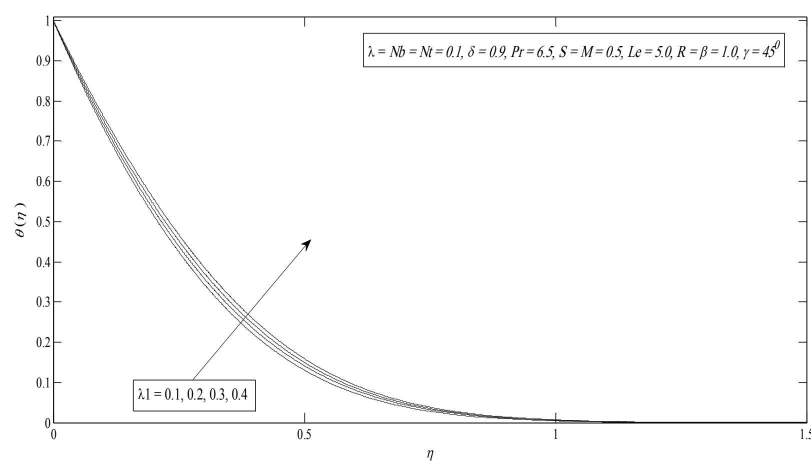

Fig. 20. Temperature profile for several values of λ_1

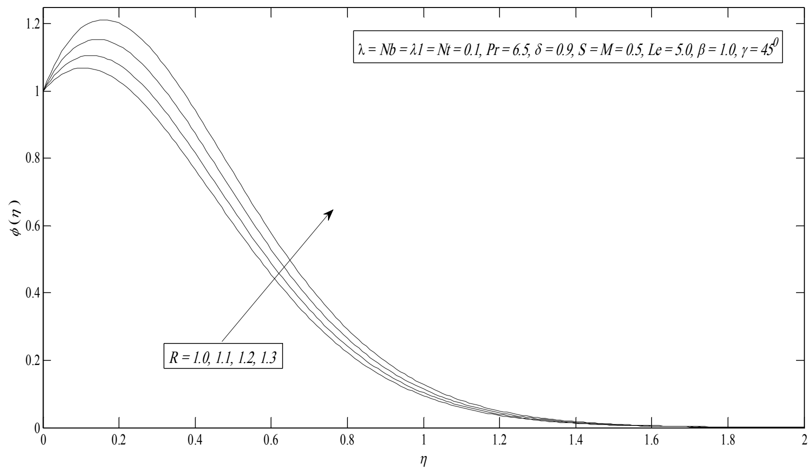

Fig. 21. Concentration profile for several value of *R*

4 Conclusions

In progress, the problem is explored the heat and mass exchange of Casson nanofluid flow above porous linear slanted extending sheet. The main conclusions are the following:

- The Nusselt number decreases by enhancing the heat generation or absorption parameter.
- The temperature profile upturns for large values of the heat generation or absorption parameter.
- The temperature curve increases by improving the Brownian motion factor.
- The velocity profile drop for bigger values of the suction parameter.
- The boundary layer thickness reduces by increasing the values of the Prandtl number.
- It is noted that for changed values of Casson constraint velocity contour drops.

Competing Interests

Authors have declared that no competing interests exist.

References

[1]. Khan WA, Pop I. Boundary-layer flow of a nanofluid past a stretching sheet. International Journal of Heat and Mass Transfer. 2010;53(11):2477–2483.

[2]. Choi SUS, Singer DA, Wang HP. Developments and applications of non-Newtonian flows. ASME FED. 1995;66:99–105.

[3]. Eastman JA, Choi US, Li S, Thompson LJ, Lee S. Enhanced thermal conductivity through the development of nanofluids. MRS Online Proceedings Library Archive. 1996;457.

[4]. Buongiorno J. Convective transport in nanofluids. Journal of Heat Transfer. 2006;128(3):240–250.

[5]. Anwar MI, Shafie S, Hayat T, Shehzad SA, Salleh MZ. Numerical study for MHD stagnation-point flow of a micropolar nanofluid towards a stretching sheet. Journal of the Brazilian Society of Mechanical Sciences and Engineering. 2017;39(1):89–100.

[6]. Mitra A. Computational modelling of boundary-layer flow of a nano fluid over a convective heated inclined plate. Journal of Mechanics of Continua and Mathematical Sciences. 2018;13(2):88-94.

[7]. Khan M, Shahid A, Malik MY, Salahuddin T. Thermal and concentration diffusion in Jeffery nanofluid flow over an inclined stretching sheet: A generalized Fourier's and Fick's perspective. Journal of Molecular Liquids. 2018;251:7–14.

[8]. Hatami M, Jing D, Yousif MA. Three-dimensional analysis of condensation nanofluid film on an inclined rotating disk by efficient analytical methods. Arab Journal of Basic and Applied Sciences. 2018;25(1):28–37.

[9]. Govindarajan A. Radiative fluid flow of a nanofluid over an inclined plate with non-uniform surface temperature. In Journal of Physics: Conference Series. IOP Publishing. 2018;1000(1):012173.

[10]. Chakraborty T, Das K, Kundu PK. Ag-water nanofluid flow over an inclined porous plate embedded in a non-Darcy porous medium due to solar radiation. Journal of Mechanical Science and Technology. 2017;31(5):2443-2449.

[11]. Ziaei-Rad M, Kasaeipoor A, Rashidi MM, Lorenzini G. A similarity solution for mixed-convection boundary layer nanofluid flow on an inclined permeable surface. Journal of Thermal Science and Engineering Applications. 2017;9(2):021015.

[12]. Thumma T, Bég OA, Sheri SR. Finite element computation of magnetohydrodynamic nanofluid convection from an oscillating inclined plate with radiative flux, heat source and variable temperature effects. Proceedings of the Institution of Mechanical Engineers, Part N: Journal of Nanomaterials, Nanoengineering and Nanosystems. 2017;231(4):179-194.

[13]. Mebarek-Oudina F. Convective heat transfer of Titania nanofluids of different base fluids in cylindrical annulus with discrete heat source. Heat Transfer—Asian Research. 2019;48(1):135-147.

[14]. Hamrelaine S, Mebarek-Oudina F, Sari MR. Analysis of MHD Jeffery Hamel flow with suction / injection by homotopy analysis method. Journal of Advanced Research in Fluid Mechanics and Thermal Sciences. 2019;58(02):173-186.

[15]. Raza J, Farooq M, Mebarek-Oudina F, Mahanthesh B. Multiple slip effects on MHD non-Newtonian nanofluid flow over a nonlinear permeable elongated sheet. Multidiscipline Modeling in Materials and Structures; 2019.

[16]. Ahmmed SF, Biswas R, Afikuzzaman M. Unsteady magnetohydrodynamic free convection flow of nanofluid through an exponentially accelerated inclined plate embedded in a porous medium with variable thermal conductivity in the presence of radiation. Journal of Nanofluids. 2018;7(5):891-901.

[17]. Biswas R, Ahmmed SF. Effects of hall current and chemical reaction on magnetohydrodynamics unsteady heat and mass transfer of casson nanofluid flow through a vertical plate. Journal of Heat Transfer. 2018;140(9):092402.

[18]. Biswas R, Hasan M, Mondal M, Shanchia K, Bulbul M, Ahmmed SF. A numerical superintendence with stability exploration of casson nanofluid flow in the effects of variable thermal conductivity and radiation. Advanced Science, Engineering and Medicine. 2019;11(8):697-707.

[19]. Kumar MS, Sandeep N, Kumar BR, Saleem S. A comparative study of chemically reacting 2D flow of Casson and Maxwell fluids. Alexandria Engineering Journal; 2017.

[20]. Shaw S, Mahanta G, Sibanda P. Non-linear thermal convection in a Casson fluid flow over a horizontal plate with convective boundary condition. Alexandria Engineering Journal. 2016;55(2):1295–1304.

[21]. Ali M, Aruna G, Raju RS. MHD boundary layer Casson fluid flow over a vertically inclined plate: Grid study and convergence analysis of finite element technique. Journal of Nanofluids. 2018;7(6): 1195-1207.

[22]. Vijayaragavan R, Kavitha MA. Heat and mass transfer in unsteady MHD Casson fluid flow past an inclined plate with thermal radiation and heat source/sink. Research Journal of Engineering and Technology. 2018;9(2):214–233.

[23]. Shamshuddin MD, Mishra SR, Thumma T. Chemically reacting radiative Casson fluid over an inclined porous plate: A numerical study. In Numerical Heat Transfer and Fluid Flow. Springer, Singapore. 2019;469-479.

[24]. Biswas R, Mondal M, Sarkar DR, Ahmmed SF. Effects of radiation and chemical reaction on MHD unsteady heat and mass transfer of Casson fluid flow past a vertical plate. Journal of Advances in Mathematics and Computer Science. 2017;1-16.

[25]. Manideep P, Raju RS, Rao TSN, Reddy GJ. Unsteady MHD free convection flow of casson fluid over an inclined vertical plate embedded in a porous media. In AIP Conference Proceedings. AIP Publishing. 2018;1953(1):140038.

[26]. Raju RS, Reddy BM, Reddy GJ. Finite element solutions of free convective Casson fluid flow past a vertically inclined plate submitted in magnetic field in presence of heat and mass transfer. International Journal for Computational Methods in Engineering Science and Mechanics. 2017; 18(4-5):250-265.

[27]. Vijayaragavan R, Kavitha MA. Heat and mass transfer in unsteady MHD Casson fluid flow past an inclined plate with thermal radiation and heat source/sink. Research Journal of Engineering and Technology. 2018;9(2):214-223.

[28]. Prasad DK, Chaitanya GK, Raju RS. Role of casson fluid on MHD natural convective flow towards vertically inclined plate with hall current. In AIP Conference Proceedings. AIP Publishing. 2018;1953(1):140073.

[29]. Koriko OK, Oreyeni T, Omowaye AJ, Animasaun IL. Homotopy analysis of MHD free convective micropolar fluid flow along a vertical surface embedded in non-darcian thermally-stratified medium. Open Journal of Fluid Dynamics. 2016;6(3):198–221.

[30]. Jain S, Parmar A. Multiple slip effects on inclined MHD Casson fluid flow over a permeable stretching surface and a melting surface. International Journal of Heat and Technology. 2018;36(2):585-594.

[31]. Anwar I, Rahman A, Kasim M, Ismail Z, Salleh MZ, Shafie S. Chemical reaction and uniform heat generation or absorption effects on MHD stagnation-point flow of a nanofluid over a porous sheet. 2013;24(10):1390–1398.
Available:https://doi.org/10.5829/idosi.wasj.2013.24.10.1307

[32]. Shit GC, Majee S. Hydromagnetic flow over an inclined non-linear stretching sheet with variable viscosity in the presence of thermal radiation and chemical reaction. Journal of Applied Fluid Mechanics. 2014;7(2).

[33]. Eid MR. Chemical reaction effect on MHD boundary-layer fl ow of two-phase nano fl uid model over an exponentially stretching sheet with a heat generation. Journal of Molecular Liquids. 2016;220:718–725.
Available:https://doi.org/10.1016/j.molliq.2016.05.005

[34]. Malik MY. Effects of second order chemical reaction on MHD free convection dissipative fluid flow past an inclined porous surface by way of heat generation : A lie group analysis 1 introduction 2 Flow analysis. 2016;45(2):35–45.

[35]. Bohra S. Heat and mass transfer over a three-dimensional inclined non-linear stretching sheet with convective boundary conditions. Indian Journal of Pure & Applied Physics (IJPAP). 2017;55(12): 847-856.

[36]. Sheri SR, Modugula P. Thermal-diffusion and diffusion-thermo effects on MHD flow through porous medium past an exponentially accelerated inclined plate with variable temperature. ARPN Journal of Engineering and Applied Sciences. 2017;12(19):5518–5526.
Available:https://doi.org/10.1016/j.asej.2015.08.014

[37]. Biswas R, Mondal M, Islam A. A steady MHD natural convection and heat transfer fluid flow through a vertical surface in the existence of hall current and radiation. Instrumentation, Mesure, Metrologie. 2018;17(2):331.

[38]. Mebarek-Oudina F. Numerical modeling of the hydrodynamic stability in vertical annulus with heat source of different lengths. Engineering Science and Technology, An International Journal. 2017;20(4):1324-1333.

[39]. Biswas R, Mondal M, Shanchia K, Ahmed R, Samad S, Ahmmed SF. Explicit finite difference analysis of an unsteady magnetohydrodynamics heat and mass transfer micropolar fluid flow in the presence of radiation and chemical reaction through a vertical porous plate. Journal of Nanofluids. 2019;8(7):1583-1591.

[40]. Biswas R, Mondal M, Hossain S, Urmi KF, Suma UK, Katun M. A numerical investigation with hydromagnetic stability convergence analysis on unsteady heat and mass transfer fluid flow through a vertical porous plate. Advanced Science, Engineering and Medicine. 2019;11(8):687-696.

[41]. Biswas R, Mondal M, Shanchia K, Ahmed R, Samad S, Ahmmed SF. Explicit finite difference analysis of an unsteady magnetohydrodynamics heat and mass transfer micropolar fluid flow in the presence of radiation and chemical reaction through a vertical porous plate. Journal of Nanofluids. 2019;8(7):1583-1591.

Peer-review history:
The peer review history for this paper can be accessed here (Please copy paste the total link in your browser address bar)
http://www.sdiarticle3.com/review-history/50499